Original Article

Kurume Medical Journal, 66, 217-224, 2019

Comparison of Structural Properties Between Postnatal and Adult Tendon Insertion with FIB/SEM Tomography in Rat

TAKU YAMADA*, TOMONOSHIN KANAZAWA*,**, KEISUKE OHTA* AND KEI-ICHIRO NAKAMURA*

**Division of Microscopic and Development Anatomy, Department of Anatomy,*
***Department of Orthopaedic surgery, Kurume University School of Medicine, Kurume 830-0011, Japan*

Received 2 October 2019, accepted 25 November 2019
J-STAGE advance publication 25 October 2021

Edited by KIMIAKI SATO

Summary: ***Objective*:** The repaired tendon-bone interface after rotator cuff (RC) repair has been identified as a mechanical weak point, which may contribute to re-tearing. Analyzing the postnatal development of a normal tendon insertion in detail may be useful in helping to promote the regeneration of a normal tendon insertion. We verified the morphological differences between postnatal and adult tendon insertions in terms of the cellular structural properties using FIB/SEM tomography.

***Materials and Method*:** SPostnatal and adult Sprague–Dawley rats were used as a model of tendon insertion. The morphological structure of the insertion was evaluated using hematoxylin and eosin (HE) staining, and the 3D ultrastructure of the cells in the insertion was evaluated using FIB/SEM tomography. Additionally, the volume of the cell bodies, nuclei, and cytoplasm were measured and compared in a quantitative analysis.

***Results*:** On conventional histology, the boundary line between the fibrocartilage and mineralized cartilage was flat in the adult insertions; however, the boundary line between the mineralized cartilage and bone formed deep interdigitations. The morphology of the cells among the collagen bundles in the adult insertions was completely different from those in the postnatal insertions at the 3D ultrastructural level. The cellular structural properties were statistically different between the postnatal and adult insertions.

***Conclusions*:** In the present study, the morphological differences between postnatal and adult tendon insertion in terms of the ultrastructural cellular properties were clarified. These findings may aid in determining how to regenerate a clinically stable tendon insertion at the tendon-bone interface after RC repair.

Keywords rotator cuff, tendon insertion, FIB/SEM tomography

INTRODUCTION

A rotator cuff (RC) tear is a common soft tissue injury of the shoulder joint. Although surgical repair has become the primary treatment for RC tears, the failure rate of RC repair ranges from 5-57% [1,2]. The repaired tendon-bone interface has been identified as a mechanical weak point [3], which may contribute to re-tearing. Therefore, it is fundamentally necessary to clarify the numerous factors that affect tendon-to-bone healing after RC repair.

It is well known that the histological structure of the repaired tendon-bone interface is completely different from that of a normal tendon insertion. In a normal tendon insertion, the tendon attaches to the bone via fibrocartilage tissue, which consists of four zones: the tendon, fibrocartilage, mineralized cartilage, and bone [4,5]. These structures functionally transfer the stress between the dissimilar materials [6]. Additionally, the transition from the mineralized cartilage to the tendon is gradual and continuous, and there is no clearly defined boundary between the zones, especial-

Corresponding Author: Kei-ichiro Nakamura, Division of Microscopic and Development Anatomy, Department of Anatomy, Kurume University School of Medicine, 67 Asahi-machi, Kurume, Fukuoka. 830-0011, Japan. Tel: +81-942-31-7528, Fax: +81-942-32-7528, E-mail: ana2nkmr@med.kurume-u.ac.jp

Abbreviations: 3D, three-dimensional; FIB/SEM, Focused Ion Beam/Scanning Electron Microscope; HE, hematoxylin; RC, rotator cuff.

ly at the ultrastructural level [7]. These structures act as a shock absorber by reducing the stiffness gradient, and also contribute to a reduction in the tendon angulation so that further shear stress does not occur.

In contrast, the repaired tendon anchors to the bone via fibro-vascular tissue rather than via the regeneration of the fibrocartilaginous insertion [3,6]. The mechanical properties of the repaired tendon-bone interface cannot reach a normal physiological level, and histologically, a clear boundary is evident between the tendon and bone. These morphological alterations can result in biological instability after RC repair [8].

Analyzing the postnatal development of a normal tendon insertion in detail may provide insights into the regeneration of a normal tendon insertion at the repaired tendon-bone interface after RC repair. Thus, several researchers have already studied the development of normal insertions [9-16]. However, the differences in the cellular structural properties between postnatal and adult insertions at the ultrastructural level have not yet been clarified. A better understanding of these ultrastructural properties would help in determining ways to reduce the occurrence of re-tears.

Although conventional electron microscopy has provided a detailed description of the ultrastructure of a normal tendon insertion, it has been impossible to gauge the morphological structure of the entire region of a normal tendon insertion at electron microscopic resolution, and three-dimensional (3D) information has also been limited because the analysis is only done using a number of single sections.

Recently the development and introduction of focused ion beam/scanning electron microscope (FIB/SEM) tomography render it possible to analyze a wider area with a higher resolution at the ultrastructure level, as fine ablation could be performed by FIB to obtain a flat surface, even for hard tissue like bones. In addition, the serial stack images allow for the reconstruction of the 3D ultrastructure of cells [7,17-20], and this has led to an improved understanding of the fine morphology and development of normal tendon insertion. Moreover, each serial stack image can be used to quantitatively analyze the ultrastructural properties of the cells at the tendon insertion. FIB/SEM tomography can analyze the 3D ultrastructure of cells at the transmission electron microscopic level. Moreover, each serial stack image can be used to quantitatively analyze the structural properties of the cells at the tendon insertion at the ultrastructural level.

In the present study, we clarified the morphological differences between postnatal and adult tendon insertions in terms of the cellular structural properties using 3D reconstructed ultrastructural image obtained by FIB/SEM tomography.

MATERIALS AND METHODS

Study Design:

This study was approved by the ethics review board of the Kurume University Animal Care Center. Postnatal Sprague–Dawley rats (aged 1 week; postnatal tendon insertions) and adult Sprague-Dawley rats (aged 12 week; weight, 510-550 g; adult tendon insertions) were used as a model of normal tendon insertion. In total, six rats were sacrificed, and shoulders of both the right and left side were removed. The morphological structure of the normal insertion was evaluated using hematoxylin and eosin (HE) staining under a light microscope, and the 3D ultrastructure of the cells was evaluated using FIB/SEM tomography. Additionally, the volume of the whole cell bodies, nuclei, and cytoplasm in each experimental group were measured and compared in a quantitative analysis (Fig. 1).

Conventional histology:

After removal of the supraspinatus tendon-humerus complex, the specimens were fixed in 4% buffered formalin. In adult insertions, specimens were additionally decalcified with Kalkitox solution (Wako Pure Chemical Industries, Ltd., Osaka, Japan). The specimens were embedded in paraffin and cut into 5-μm thick sections. The slides were stained with HE. The specimens were visualized under a light microscope (BZ-X710; Keyence, Osaka, Japan) and photomicrographs were obtained.

FIB/SEM tomography

Sprague-Dawley rats were deeply anesthetized with diethyl ether and sodium pentobarbital, transcardially perfused through the left ventricle with heparin-containing saline, and subsequently fixed with half Karnovsky solution (2% paraformaldehyde, 2.5% glutaraldehyde, and 2 mM CaCl2 in 0.1 M cacodylate buffer). After perfusion fixation, the supraspinatus tendon-humerus complexes were harvested and further immersed in the same fixative for 2 h at 4°C. After decalcification with 5% EDTA solution for the adult insertions, the specimens were cut into small cubes and further fixed with 2% ferrocyanide and 1% OsO_4. Subsequently, the specimens were treated with 1% thiocarbohydrazide and then immersed in a 1% OsO_4 solution. For en bloc staining, the specimens were immersed in a solution of 4% uranyl acetate so-

lution overnight and finally washed with distilled water. The specimens were further en bloc stained with Walton's lead aspartate solution. They were then dehydrated with a graded ethanol series, infiltrated with an epoxy resin mixture, and polymerized at 60°C for 72 h. The surface of each embedded specimen was exposed with a diamond knife, and the resin blocks were trimmed and placed on an appropriate holder. Each specimen was fixed to the stage of the FIB/SEM machinery (Quanta 3DFEG; FEI, Hillsboro, OR, USA). Serial images of the block face were acquired by repeated cycles of sample surface milling using a focused gallium ion beam (milling step: 100 nm, 700 cycles) and by image acquisition using SEM as a compositional contrast image from secondary electrons (landing energy, 2.5 keV). The reconstructed images covered the supraspinatus tendon insertion. Approximately 700 block face images could be obtained per specimen. The morphology of the cells was evaluated after 3D reconstruction using Amira 5.5 software (FEI). The 3D morphology of the cells was extracted using a semi-manual procedure [7,8,21,22]. Briefly, all image stacks ware normalised using a histogram-based image filter, and a median filter was applied to prepare for threshold segmentation. The cellular regions ware selected using the threshold method; irregular regions in the selected regions were manually removed [8].

Quantitative analysis of the structural properties on FIB/SEM tomography

After reconstruction, we performed a quantitative analysis of the whole cells within the evaluated area. First, we reconstructed 93 cells in postnatal insertions and 58 cells in adult insertions. Subsequently, we excluded 37 cells in postnatal insertions and 27 cells in adult insertions because the cell bodies were partly outside the reconstructed range, and we could not track the entire body of these cells. Thus, we included 56 cells in postnatal insertions and 31 cells in adult insertions in the quantitative analysis. The volumes of each cell body and nucleus were measured. Additionally, the total cell volume, nuclei volume, cytoplasmic volume, and also cytoplasmic-total cell volume ratio were calculated using Amira software (Fig. 2). These structural properties were compared between postnatal and adult insertions.

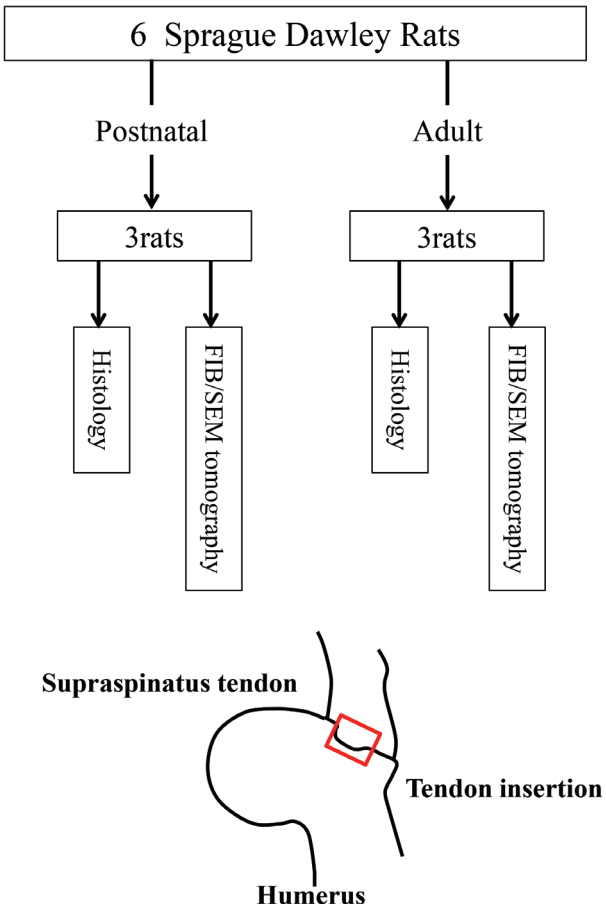

Fig. 1. Diagram of study design: Six rats were sacrificed, and both the right and left shoulders were removed. The morphological structure of the normal insertion was evaluated using hematoxylin and eosin (HE) staining, and the 3D ultrastructure of the cells in the normal insertion was evaluated using FIB/SEM tomography.

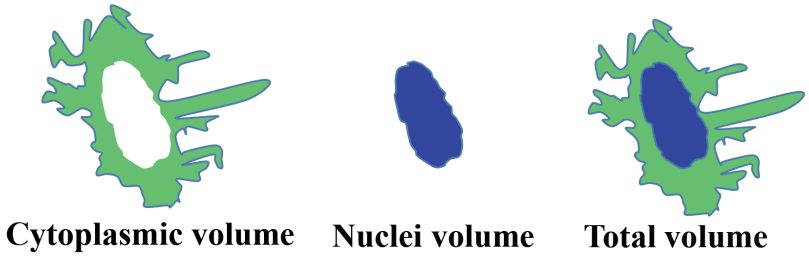

Fig. 2. Cytoplasmic volume (green), nuclei volume (blue), and total volume (green and blue). Cytoplasmic to total volume ratio were calculated using Amira software.

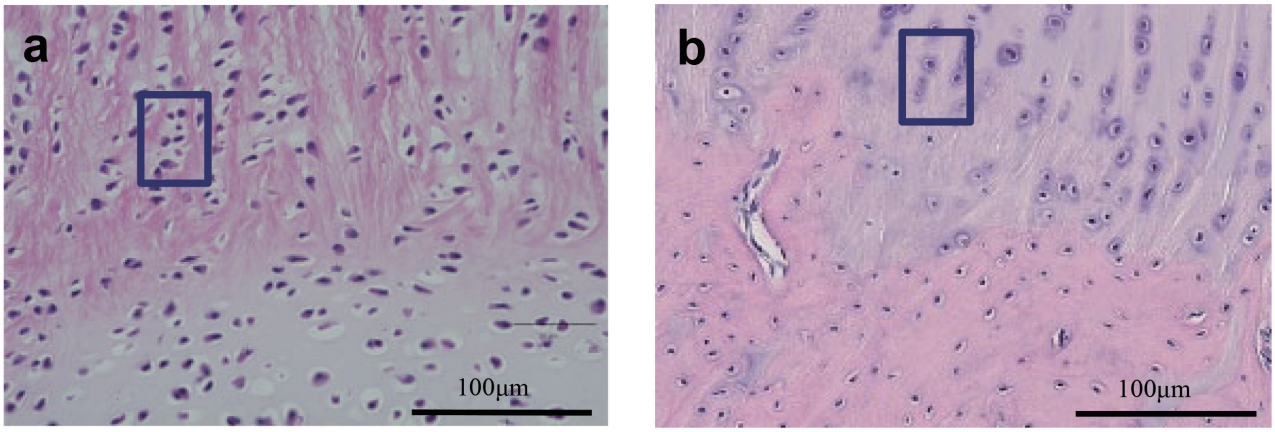

Fig. 3. Histological micrograph of the tendon insertion (HE staining): (a) The boundary line between the immature collagen bundles and epiphyseal nuclei was flat. (b) The boundary line between the mineralized cartilage and the bone formed deep interdigitations. The blue rectangular frames in each micrograph indicate the areas equivalent to those in Fig. 4a & b, respectively.

Statistical analysis:

Statistical analyses were performed using JMP version 13 software (SAS Institute INC., Cary, USA). Data are expressed as means and standard deviations. The Wilcoxon test was used to evaluate differences in structural properties between postnatal and adult insertions. P values <0.05 were considered statistically significant. These data were shown as Box-and-whisker graphs.

RESULTS

Conventional histology

In postnatal insertions, the immature collagen bundles were directly attached to the epiphyseal nuclei, and their boundary was clearly identified. Additionally, the boundary line between the immature collagen bundles and epiphyseal nuclei was flat but not interdigitated (Fig. 3a). In the tendon midsubstance/insertion, spherical cells, in columnar formation, were observed between the immature collagen bundles (Fig. 3b). In the epiphyseal nuclei, typical chondroid cells were evident [22]. On the other hand, matured collagen bundles were solidly attached to the bone tissue in adult insertions. The boundary line between the fibrocartilage and mineralized cartilage was also flat, similar to that in the postnatal insertions. However, the boundary line between the mineralized cartilage and the bone formed deep interdigitations. Fibro-cartilage-like cells, in columnar formation, were located between the matured collagen bundles. The cells became more spherical toward the bone side. These structures in adult insertions looked similar to previous descriptions [4,5].

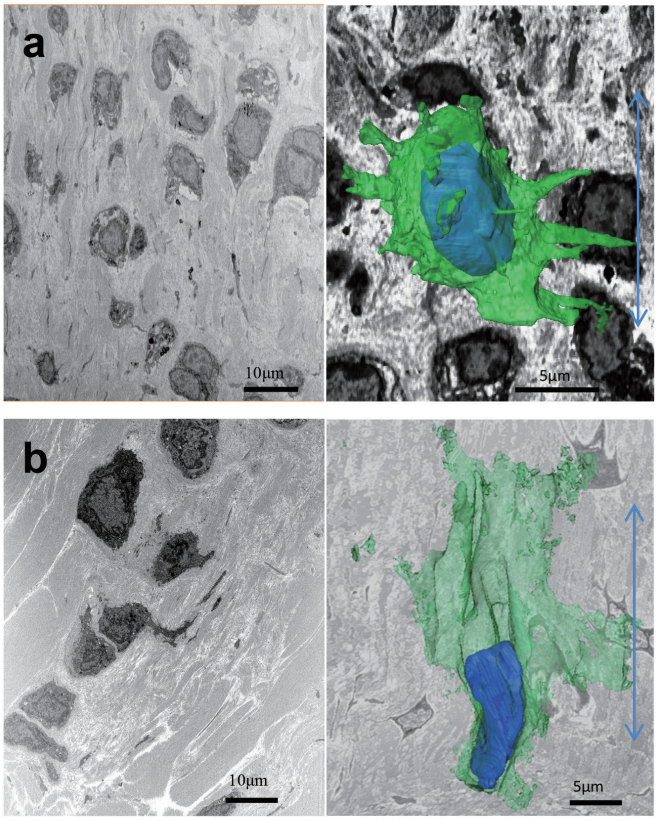

Fig. 4. Reconstructed configurations of cells at the tendon insertion of the areas equivalent to those surrounded by the blue rectangular frame in Fig. 3.: (a) Spherical-shaped cells were irregularly localized between the loose and irregular collagen bundles in the tendon insertion. Additionally, the many cell processes had an irregular direction. (b) The cells at the insertion between the matured collagen bundles had an ellipsoidal shape. Furthermore, the direction of the cell processes was oriented to that of the adjacent collagen bundles.

3D morphology of the whole cell body on FIB/SEM tomography

In postnatal insertions, spherical cells were irregularly localized between the loose and irregular collagen bundles in the tendon insertion area. Additionally, the direction of cell processes emerging from the cell volume was irregular (Fig. 4a). In the adult insertion, the cells in the insertion area were ellipsoidal and were located between matured collagen bundles. Although the number of cell processes decreased in adult insertions, the length of each process increased. Furthermore, the orientation of the cell processes became parallel to that of the surrounding collagen bundles (Fig. 4b).

Quantitative analysis of the structural properties on FIB/SEM tomography

In total, we analyzed 56 cells in postnatal insertions and 31 cells in adult insertions in the quantitative analysis of the structural properties. The cytoplasmic volume was significantly greater in postnatal insertions (268.79±81.2μm^3) than in adult insertions (190.5±50.83μm^3; P<0.01) (Fig. 5a). Similarly, the nuclei volume was significantly greater in postnatal insertions (109.98±33.17μm^3) than in adult insertions (65.86±8.66μm^3; P<0.01) (Fig. 5b). Additionally, the total volume was significantly greater in postnatal insertions (378.77±104.73μm^3) than in adult insertions (256.36±57.68μm^3; P<0.01) (Fig. 5c). In contrast, the cytoplasmic-total volume ratio was significantly greater in the adult insertion (73.72±3.28%) than in the postnatal insertion (70.62±6.68%; P<0.01) (Fig. 5d).

DISCUSSION

The present study investigated the morphological differences between postnatal and adult tendon insertions in terms of cellular structural properties using FIB/SEM tomography. To our knowledge, this study is the first to examine the differences in cellular structural properties between postnatal and adult tendon insertions with a resolution at the transmission electron microscopic level. The main findings of the study

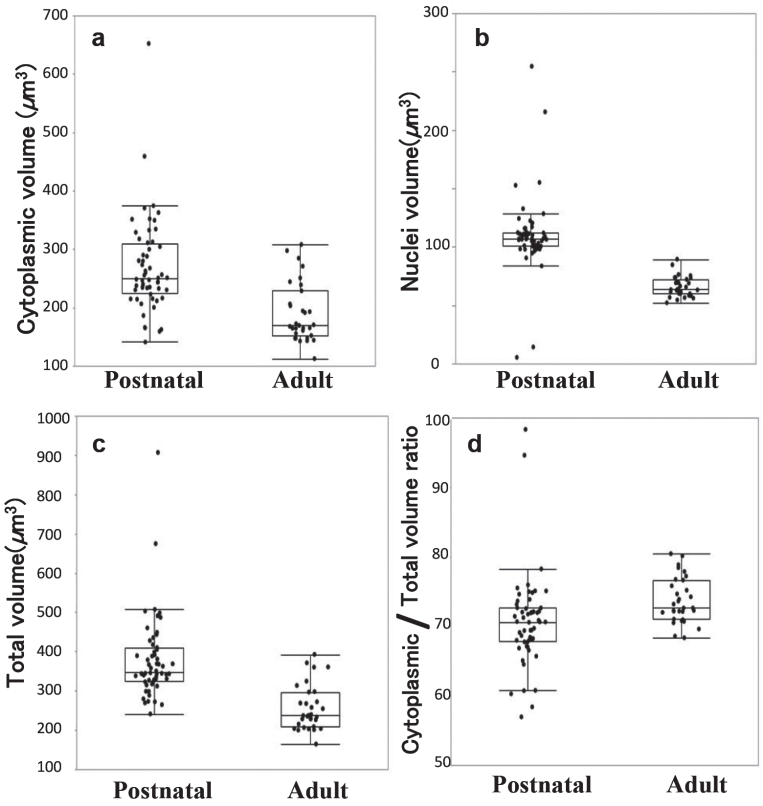

Fig. 5. Box-and-whisker diagram of cellular structural properties at the tendon insertion: (a) Cytoplasmic volume (b) Nuclei volume (c) Total volume (d) Ratio of the cytoplasm to total cell volume at tendon insertion of postnatal and adult rat large nodule of humerus.

can be summarized as follows: 1) on conventional histology, the boundary line between the immature collagen bundles and epiphyseal nuclei was flat in the postnatal insertions.

Similarly, the boundary line between the fibrocartilage and mineralized cartilage was flat in the adult insertions; however, the boundary line between the mineralized cartilage and bone formed deep interdigitations. 2) The morphology of the cells between the collagen bundles in the adult insertions was completely different from that of the postnatal insertions at the ultrastructural level. 3) The cellular structural properties (total volume, nuclei volume, cytoplasmic volume, and cytoplasmic-total volume ratio) were statistically different between the postnatal and adult insertions. Although several studies have already reported on the morphology of the tendon insertion using various histological stainings [4,5,9], few studies have described the structure of the boundary line between the mineralized cartilage and bone. In the present study, we described the structure of the boundary line between the tendon and bone in both postnatal and adult insertions. The boundary line between the immature collagen bundles and epiphyseal nuclei was flat in postnatal insertions, while the boundary line between the mineralized cartilage and the bone formed deep interdigitations in adult insertions. Thus, we have clearly demonstrated differences in the boundary line between postnatal and adult insertions. Although these structures are mechanically speculated to provide resistance against shear force, how these structures are formed remains unknown. Accordingly, the structural differences with respect to the ultrastructural level and 3D morphology need to be clarified in the future. The morphology of the cells between the collagen bundles in adult insertions was completely different from that in postnatal insertions at the ultrastructural level. Previously, we reported on the 3D ultrastructure of the cells in the tendon insertion during the first 4 postnatal weeks; the morphology of the cells drastically transformed during this period [16]. The 3D ultrastructure of the cells in the adult insertions shown in the present study was similar to that at 4 weeks postnatal in our previous report [16]. These phenomena might indicate that the transformation of the cells in the tendon insertion ceased once the collagen bundles were organized during the development of the tendon insertion. However, we have not yet analyzed whether the morphological changes resulted from cell maturation or dynamic movement. Further studies are necessary to determine the mechanism of these drastic changes. Regardless, these morphological differences in terms of the organization with respect to the collagen bundles reflect the function during tendon development.

The differences in cellular structural properties (total volume, nuclei volume, cytoplasmic volume, and cytoplasmic-total volume ratio) were statistically significant between postnatal and adult insertions. Although we previously reported on the morphology of the cells in the tendon insertion at ultrastructural level using FIB/SEM tomography [7,8,16], the present study is the first to quantitatively analyze the morphology of the cells in the tendon insertion. As a result, the total cell volume, nuclei volume, and cytoplasmic volume were found to be statistically larger in postnatal insertions than in adult insertions. Conversely, the cytoplasmic-total cell volume ratio was statistically smaller in postnatal insertions than in adult insertions. We believe that these morphological differences reflect the viability of the cells and the eventual organization of each insertion. However, future studies are needed to link the morphological differences demonstrated in the present study with the function of the cells and the development of the tendon insertion. Previously, it was impossible to quantitatively analyze cell morphology at the ultrastructural level using conventional histological methods. However, the advancement of 3D digital data obtained by FIB/SEM tomography has made it possible to quantitatively analyze the cell morphology at the ultrastructural level. Consequently, we successfully determined the differences in cell morphology between postnatal and adult insertions in terms of structural properties. In RC repair, the tendon-bone interface is repaired via the formation of fibrovascular tissue, which differs from that for the normal tendon insertion [3,8,9,23-25]. The findings of the present study could aid future research in determining how to regenerate the normal tendon insertion in the repaired tendon-bone interface after RC repair. We are planning next to verify the morphological characteristics of the cells (structural properties) in the repaired tendon-bone interface using the method of the present study.

The present study has several limitations. First, the findings obtained from these data may differ from those found in studies using human participants. However, previous reports have shown that the rat shoulder closely approximates the human shoulder in terms of anatomy [26]. Thus, the morphological differences between cells in the postnatal and adult insertions in rodent tissue could be a model of those in humans. Secondly, we simply compared the morphological differences between cells in the postnatal and adult insertions; we could not track the morphological changes

of each respective cell in the tendon insertion. These cells are an extremely important factor in preserving the mechanical transmission between dissimilar materials. Future studies are needed to clarify the morphological changes of the cell itself during tendon development. We must be cautious in interpreting the present findings, as the morphological differences may have resulted from cell maturation or movement.

Thirdly, we performed a comparative study of the morphological differences of the cells in postnatal and adult insertions using a rat model; we did not use a repair model or utilize any applications to accelerate or regenerate the tendon insertion as previously reported [27-36]. We believe our findings will benefit future studies that intend to evaluate tendon-to-bone healing utilizing various applications.

CONCLUSIONS

The present study successfully used FIB/SEM tomography to clarify the differences in morphology and cellular structural properties between postnatal and adult tendon insertions.

These findings can aid in determining how to regenerate a normal tendon insertion in the repaired tendon-bone interface after RC repair.

COMPETING INTERESTS: The authors have no conflicts of interest directly relevant to the content of this article.

ACKNOWLEDGMENTS: This work was supported by JSPS KAKENHI Grant Number 17K11038. We would also like to thank all the microscopic and development anatomy staff that gave us advice.

REFERENCES

1. Franceschi F, Ruzzini L, Longo UG, Martina FM, Zobel BB et al. Equivalent Clinical Results of Arthroscopic Single-Row and Double-Row Suture Anchor Repair for Rotator Cuff Tears: A Randomized Controlled Trial. Am J Sports Med 2007; 35:1254-1260.
2. Zumstein MA, Jost B, Hempel J, Hodler J, and Gerber C. The Clinical and Structural Long-Term Results of Open Repair of Massive Tears of the Rotator Cuff. J Bone Joint Surg Am 2008; 90:2423-2431.
3. Rodeo SA, Arnoczky SP, Torzilli PA, Hidaka C, and Warren RF. Tendon-healing in a bone tunnel. A biomechanical and histological study in the dog. J Bone Joint Surg Am 1993; 75:1795-1803.
4. Benjamin M, Evans EJ, and Copp L. The histology of tendon attachments to bone in man. J Anat 1986; 149:89-100.
5. Cooper RR and Misol S. Tendon and ligament insertion. A light and electron microscopic study. J Bone Joint Surg Am 1970; 52:1-20.
6. Lu HH and Thomopoulos S. Functional Attachment of Soft Tissues to Bone: Development, Healing, and Tissue Engineering. Ann Rev Biome Eng 2013; 15:201-226.
7. Kanazawa T, Gotoh M, Ohta K, Shiba N, and Nakamura K. Novel characteristics of normal supraspinatus insertion in rats: an ultrastructural analysis using three-dimensional reconstruction using focused ion beam/scanning electron microscope tomography. Muscles Ligaments Tendons J 2014; 4:182-187.
8. Kanazawa T, Gotoh M, Ohta K, Honda H, Ohzono H et al. Histomorphometric and ultrastructural analysis of the tendon-bone interface after rotator cuff repair in a rat model. Sci Rep 2016; 6:33800.
9. Thomopoulos S, Genin GM, and Galatz LM. The development and morphogenesis of the tendon-to-bone insertion - what development can teach us about healing. J Musculoskelet Neuronal Interact 2010; 10:35-45.
10. Galatz L, Rothermich S, VanderPloeg K, Petersen B, Sandell L et al. Development of the supraspinatus tendon-to-bone insertion: localized expression of extracellular matrix and growth factor genes. J Orthop Res 2007; 25:1621-1628.
11. Nawata K, Minamizaki T, Yamashita Y, and Teshima R. Development of the attachment zones in the rat anterior cruciate ligament: changes in the distributions of proliferating cells and fibrillar collagens during postnatal growth. J Orthop Res 2002; 20:1339-1344.
12. Schwartz AG, Pasteris JD, Genin GM, Daulton TL, and Thomopoulos S. Mineral Distributions at the Developing Tendon Enthesis. PLoS One 2012; 7:e48630.
13. Thomopoulos S, Kim HM, Rothermich SY, Biederstadt C, and Das R. Decreased muscle loading delays maturation of the tendon enthesis during postnatal development. J Orthop Res 2007; 25:1154-1163.
14. Kjaer M. Role of Extracellular Matrix in Adaptation of Tendon and Skeletal Muscle to Mechanical Loading. Physiol Rev 2004; 84:649-698.
15. Fujioka H, Wang GJ, Mizuno K, Balian G, and Hurwitz SR. Changes in the expression of type-X collagen in the fibrocartilage of rat Achilles tendon attachment during development. J Orthop Res 1997; 15:675-681.
16. Kanazawa T, Gotoh M, Ohta K, Shiba N, and Nakamura K. Three-dimensional ultrastructural analysis of development at the supraspinatus insertion by using focused ion beam/scanning electron microscope tomography in rats. J Orthop Res 2016; 34:969-976.
17. Ichimura K, Miyazaki N, Sadayama S, Murata K, Koike M et al. Three-dimensional architecture of podocytes revealed by block-face scanning electron microscopy. Sci Rep 2015; 5:8993.
18. Ohta K, Sadayama S, Togo A, Higashi R, Tanoue R et al. Beam deceleration for block-face scanning electron microscopy of embedded biological tissue. Micron 2012; 43:612-620.
19. Schneider P, Meier M, Wepf R, and Müller R. Serial FIB/SEM imaging for quantitative 3D assessment of the osteocyte lacuno-canalicular network. Bone 2011; 49:304-311.
20. Knott G, Marchman H, Wall D, and Lich B. Serial section scanning electron microscopy of adult brain tissue using

focused ion beam milling. The Journal of neuroscience : J Neurosci 2008; 28:2959-2964.
21. Hirashima S, Ohta K, Kanazawa T, Uemura K, Togo A et al. Anchoring structure of the calvarial periosteum revealed by focused ion beam/scanning electron microscope tomography. Sci Rep. 2015; 5, 17511.
22. Kanazawa T, Gotoh M, Ohta K, Shiba N, and Nakamura K. Three-dimensional ultrastructural analysis of development at the supraspinatus insertion by using focused ion beam/scanning electron microscope tomography in rats. J Orthop Res 2015; 34, 969–976.
23. Thomopoulos S, Williams GR, and Soslowsky LJ. Tendon to Bone Healing: Differences in Biomechanical, Structural, and Compositional Properties Due to a Range of Activity Levels. J biomech Eng 2003; 125:106-113.
24. Aoki M, Oguma H, Fukushima S, Ishii S, Ohtani S et al. Fibrous connection to bone after immediate repair of the canine infraspinatus: The most effective bony surface for tendon attachment. J Shoulder Elbow Surg 2001; 10:123-128.
25. Kanazawa T, Soejima T, Murakami H, Inoue T, Katouda M et al. An immunohistological study of the integration at the bone-tendon interface after reconstruction of the anterior cruciate ligament in rabbits. J Bone Joint Surg Br 2006; 88:682-687.
26. Soslowsky LJ, Carpenter JE, DeBano CM, Banerji I, and Moalli MR. Development and use of an animal model for investigations on rotator cuff disease. J Shoulder Elbow Surg 1996; 5:383-392.
27. Hettrich CM, Beamer BS, Bedi A, Deland K, Deng XH et al. The Effect of rhPTH on the Healing of Tendon to Bone in a Rat Model. J Orthop Res 2011; 30:769-774.
28. Gulotta LV, Kovacevic D, Packer JD, Deng XH, and Rodeo SA. Bone Marrow-Derived Mesenchymal Stem Cells Transduced With Scleraxis Improve Rotator Cuff Healing in a Rat Model. Am J Sports Med 2011; 39:1282-1289.
29. Walsh WR, Stephens P, Vizesi F, Bruce W, Huckle J et al. Effects of Low-Intensity Pulsed Ultrasound on Tendon-Bone Healing in an Intra-articular Sheep Knee Model. Arthroscopy 2007; 23:197-204.
30. Thomopoulos S, Matsuzaki H, Zaegel M, Gelberman RH, and Silva MJ. Alendronate prevents bone loss and improves tendon-to-bone repair strength in a canine model. J Orthop Res 2007; 25:473-479.
31. Ouyang HW, Goh JC, and Lee EH. Use of Bone Marrow Stromal Cells for Tendon Graft-to-Bone Healing: Histological and Immunohistochemical Studies in a Rabbit Model. Am J Sports Med 2004; 32:321-327.
32. Martinek V, Latterman C, Usas A, Abramowitch S, Woo SL et al. Enhancement of Tendon-Bone Integration of Anterior Cruciate Ligament Grafts with Bone Morphogenetic Protein-2 Gene Transfer: A Histological and Biomechanical Study. J Bone Joint Surg Am 2002; 84:1123-1131.
33. Rodeo SA, Suzuki K, Deng XH, Wozney J, and Warren RF. Use of Recombinant Human Bone Morphogenic Protein-2 to Enhance Tendon Healing in a Bone Tunnel. Am J Sports Med 1999; 27:476-488.
34. Mutsuzaki H, Sakane M, Nakajima H, and Ochiai N. Calcium phosphate-hybridised tendon graft to reduce bone-tunnel enlargement after ACL reconstruction in goats. Knee 2012; 19:455-460.
35. Kanazawa T, Soejima T, Noguchi K, Tabuchi K Noyama M et al. Tendon-to-bone healing using autologous bone marrow-derived mesenchymal stem cells in ACL reconstruction without a tibial bone tunnel-A histological study. Muscles Ligaments Tendons J 2014; 4:201-206.
36. Lovric V, Chen D, Yu Y, Oliver RA, Genin F et al. Effects of Demineralized Bone Matrix on Tendon-Bone Healing in an Intra-articular Rodent Model. Am J Sports Med 2012; 40:2365-2374.